Altered serum profiles in guinea pigs with allergic asthma after acupoint sticking therapy: New insights from a metabolomics approach

Shi-jian Xiang[a#], Meng-heng Li[d#], Chi-on Chan[b,d], Qun Shen[a], Si-bao Chen[b,d], Bai-chao An[a], Ailsa Chui-ying Yuen[b,d], Wen-feng Wu[a], Hok-him Tang[d], Si-wei Cao[a], Shi-fa Ruan[a], Zhu-xian Wang[a], Li-dong Weng[a], Hong-xia Zhu[c], Huo-ji Chen[a], Melody Yee-Man Wong[f], Yan Zhang[e], Daniel Kam-wah Mok[b,d]*, Qiang Liu[a]*

a. School of Traditional Chinese Medicine, Southern Medical University, Guangzhou, 510515, China.
b. State Key Laboratory of Chinese Medicine and Molecular Pharmacology (Incubation), Shenzhen 518057, China
c. Integrated Hospital of Traditional Chinese Medicine, Southern Medical University, Guangzhou, 510315, China.
d. Department of Applied Biology and Chemical Technology, The Hong Kong Polytechnic University, Hong Kong, China
e. Spine Disease Research Institute, Longhua Hospital, Shanghai University of Traditional Chinese Medicine, Shanghai 200032, China
f. University Research Facility in Chemical and Environmental Analysis, The Hong Kong Polytechnic University, Hong Kong, China

#Shi-jian Xiang[#] and Meng-heng Li[#] contributed equally to this work.

*Corresponding author. School of Traditional Chinese Medicine, Southern Medical University, Guangzhou, 510515, China. Tel.: +86-20-6164-8264, *Email-address*: gzlq2002@163.com (Qiang Liu)
*Corresponding author. Department of Applied Biology and Chemical Technology, The Hong Kong Polytechnic University, Hong Kong, China. Tel.: +852 3400 8681; fax: 23649932, *Email-address*:bcdaniel@polyu.edu.hk (Daniel Kam-Wah Mok).

Abstract

Background: Clinical evidence gathered in Chinese communities suggested that acupoint sticking therapy could be an alternative treatment for asthma-related diseases. However, its underlying mechanism is still poorly understood.

Aim/hypothesis: In this study, we aimed to investigate the mechanism of the anti-inflammatory effect of acupoint sticking application with 'Treatment of Winter Disease in Summer' (TWDS) prescription by using metabolomics.

Methods: Allergic asthma in guinea pig was sensitized and challenged by ovalbumin (OVA). Histopathological evaluation of the lung tissue was performed by hematoxylin and eosin (H&E) staining and Masson's trichrome staining. The levels of Th1/Th2 cytokine and IgE level in serum were measured using enzyme-linked immunoassay

(ELISA). The mRNA expression levels of IL-4, IL-5, IL-13 and orosomucoid-like 3 (ORMDL3) were measured using quantitative reverse transcription polymerase chain reaction (RT-qPCR). Proteins of NF-κB signaling pathway were measured using western blot.

Results: The overall results confirmed that AST with TWDS prescription had a significant protective effect against OVA-induced allergic asthma in guinea pig. This treatment not only attenuated airway inflammation and collagen deposition in the airway, but also decreased the levels of IL-4, IL-5, IL-13 and IgE in serum. In addition, metabolomics results indicated that metabolisms of phospholipid, spingolipid, purine, amino acid and level of epinephrine were restored back to the normal control level. Moreover, results of the gene expression of ORMDL3 in lung tissues indicated that AST using TWDS could alter the spingolipid metabolism. Further western blotting analysis also showed that its anti-asthmatic mechanism was via the inhibition of the NF-κB signaling pathway.

Conclusion: The study demonstrated that metabolomics provides a better understanding of the actions of TWDS acupoint sticking therapy on OVA-induced allergic asthma.

Keywords: asthma, metabolomics, NF-κB, acupoint sticking therapy, treatment of winter disease in summer prescription

Abbreviations: AST, acupoint sticking therapy; TWDS, Treatment of Winter Disease in Summer; OVA, ovalbumin; IL-4, Interleukin-4; IL-5, Interleukin-5; IL-13, Interleukin-13; ORMDL3, orosomucoid-like 3; NF-κB, Nuclear factor-kappa B; DSP, dexamethasone sodium phosphate; Th, T helper cells; IgE, Immunoglobulin E

1. Introduction

Asthma is a common chronic inflammatory respiratory disease which is generally characterized by airway hyper-responsiveness, inflammation and obstruction (Busse et al., 2001). Due to its heterogeneous syndrome encompassing a number of different subtypes and multiple phenotypes (Pavord et al., 2017), the interpretation of its underlying biological mechanism is still a challenging task. It remains a serious public health concern, affecting an estimated 300 million people worldwide (Busse et al., 2001).

Recent studies have shown that asthma is associated with immune-mediated imbalance response between T-helper type 1 (Th1) and Th2 cells. Activation of Th2 cells can help B cells to activate mast cells to release more allergic and inflammatory mediators, resulting in the elevation of the level of Immunoglobulin E (IgE) (Bosnjak et al., 2011; Larché et al., 2003). Nowadays, corticosteroids, antihistamines and leukotriene receptor antagonists are commonly used as therapeutic drugs for asthma (Chini et al., 2014). However, the side effects of these drugs have limited their use. The taking of corticosteroids in high dosages was universally found to be associated with high incidence of fractures; their long-term usage also increased the risk of myocardial infarction (Manson et al., 2009). Thus, there is an urgent need for a safe and effective alternative therapeutic treatment for asthma.

The use of acupoint sticking therapy (AST), also known as acupuncture point application therapy, in asthma management was first recorded in *Zhang Shi Yi Tong* in the Qing Dynasty (Zhang et al., 1990). AST is a treatment that works by externally applying herbal paste, which is made from different prescriptions according to treatment purposes, to acupoints. Traditionally, the powdered herbs are mixed with ginger, honey or water, covered with gauze and fixed with adhesive plaster before application to patients (Peng et al., 2012). The treatment is popular in many Chinese communities because it is non-invasive and it is often used as a preventive measure. The administration through skin is safer and could avoid first-pass metabolism of the therapeutic agent(s). This also gives a better control of the level of the therapeutic agent(s) in the blood stream (Delgadocharro and Guy, 2014). According to traditional Chinese medicine (TCM) theory, asthma is attributed to the obstruction of the lung by long-retained phlegm (Zhang et al., 2006). The lung, spleen and kidney are related to immunological functions and AST might regulate these organs through absorption of herbs and stimulation of the meridians. By using herbs with acrid-warm property and penetrating flavor, application of acupoint herbal paste might help warm the lung, remove phlegm, facilitate qi flow, dissolve masses and dredge collaterals.

Metabolomics aims at comprehensive characterization of endogenous metabolites and their variation in biological matrices such as plasma, urine and tissues by using high resolution nuclear magnetic resonance and mass spectrometry (Gorrochategui et al., 2016; Nagana Gowda et al., 2017). It is increasingly recognized as an invaluable tool to identify changes in metabolites along pathogenic development and understand the underlying mechanisms as well as influences from interventions. Metabolomics technique would provide important insights on the mechanisms of AST in the treatment of asthma disease.

Our previous work had successfully demonstrated that AST using "Treating Winter Disease in Summer' (TWDS) prescription could reduce airway hyper-responsiveness and lung inflammation in ovalbumin (OVA) - sensitized animals (Xiang et al., 2016). In the current study, we aimed to investigate the underlying mechanisms of the anti-inflammatory effect of TWDS in a guinea pig model of asthma with the use of the metabolomics approach. The results obtained here indicated that application of AST using TWDS can regulate the metabolisms of phospholipid, spingolipid, purine and amino acid. Results of the gene expression of orosomucoid-like 3 (ORMDL3) in lung tissues also indicated that AST using TWDS could alter the spingolipid metabolism. Moreover, western blotting analysis demonstrated that its anti-asthmatic mechanism was via the inhibition of the NF-κB signaling pathway. This study might provide new insights for the potential use of AST using TWDS for asthma treatment.

2. Materials and methods

2.1 Preparation of TWDS patches

TWDS prescription is composed of six Chinese Material Medica (CMMs), Sinapis Semen (*Sinapis alba* L.), Asari Radix et Rhizoma (*Asarum sieboldii* Miq.), Euphorbia kansui Radix (*Euphorbia kansui* T.N. Liou ex T.P. Wang), Corydalis Rhizoma (*Corydalis yanhusuo* W.T. Wang), Ephedra Herba (*Ephedra sinica* Stapf) and Scutellariae Radix (*Scutella baicalensis* Georgi) in a ratio of 2:2:1:2:1:1. All the CMMs above were purchased from Zhixin Herbal Pharmaceutical Company Ltd. (Guangzhou, China) and authenticated by Professor Chuanming Liu from the College of Chinese Traditional Medicine, Southern Medical University, Guangzhou, China. All the herbal materials used in our study satisfy the quality requirement of the Chinese Pharmacopoeia 2015. Details of the results of the quantitative analysis and chromatographic profiles of the herbal materials used can be found in the supplementary information. All the herbs were ground into powder and mixed with ginger juice at a 2:1 ratio to make the patches (Zhong et al., 2009).

2.2 Animals grouping, modeling and drugs administration

28 Male Hartley guinea pigs of about 275 ± 25g were obtained from the Center of Laboratory Animal Science of Guangdong (License Number SCXK GD 2014-0035, Guangzhou, China). This animal study was approved by the Ethics Committee of Southern Medical University and was conducted in compliance with the animal experiment guidelines established by The Ministry of Science and Technology of the People's Republic of China. The guinea pigs were housed in an air-conditioned room kept under the experimental condition (temperature of 25 ± 2℃, humidity of 60 ± 5% and 12/12h light/dark cycle) with free access to food and water. All guinea pigs were acclimatized for one week.

On Days 1 and 8, all guinea pigs were sensitized by intraperitoneal injection of 100 mg OVA (Grade V, purity≥98%, Sigma-Aldrich, St Louis, MO, USA) plus 1mg of aluminum hydroxide as an adjuvant in 1 mL saline. On Days 15-28, the OVA-sensitized guinea pigs were challenged by inhaling aerosol containing 1% OVA for 10min. On days 29, the challenged guinea pigs were randomly divided into 3 groups, OVA sensitization model group, dexamethasone sodium phosphate (DSP) treatment group and AST using TWDS treatment group. Normal control group animals were sensitized and challenged with aerosolized 0.9% saline (Sagar et al., 2015; Morin et al., 2013).

The DSP treatment group received intraperitoneal injection of dexamethasone sodium phosphate (0.5mg/kg, once daily). AST using TWDS treatment group received transdermal administration of TWDS patches (1g/100g, once per two days) on the acupoints of Dazhui, Feishu and Shenshu on the back. The course of treatment was 2 weeks. At the end of the treatment period (Days 43), all guinea pigs were fasted overnight, then anesthetized by intraperitoneal injection of 10% chloral hydrate anesthesia. The blood samples collected using abdominal aorta approach were centrifuged for 15min (3000 rpm/min) to obtain the serum. Serum and lung tissues were stored at -80℃ for subsequent analysis.

2.3 Chemical and Reagents

Ephedrine hydrochloride was purchased by National Institute for the Control of Pharmaceutical and Biological products of China (Beijing, China). Sinapine thiocyanate, tetrahydropalmatine, baicalin and asarinin were purchased from Chengdu Chroma-Biotech Co. Ltd. (Chengdu, China). All compounds except ephedrine hydrochloride had a purity of 98%; the purity of ephedrine hydrochloride was 99%. Glycocholic acid was purchased from Steraloids (Newport, RI, USA) while norepinephrine, epinephrine, alanine serine and valine were obtained from Sigma-Aldrich (St. Louis, MO, USA). HPLC-graded acetonitrile and methanol were obtained

from Fisher Scientific (Hampton, NH, USA). Cholic acid D_4 and formic acid were purchased from Cambridge Isotope Laboratory Inc. (Cambridge, UK) and Sigma-Aldrich (St. Louis, MO, USA), respectively. Water was purified in-house using a Milli-Q Advantage A10 water purification system (Millipore, Bedford, *MA*, USA).

2.4 Lung histopathological examination

Guinea pig lung tissues were fixed in 4% (w/v) paraformaldehyde for 24h and embedded in paraffin. A series of 4μm micro-sections were stained with Haematoxylin & Eosin (H&E) and Masson in accordance with standard protocols (Morin et al., 2011) and finally visualized under an optical microscope (LV100D, Nikon, Japan). Lung inflammation assessment was performed by semi-quantitative method (Jiao, et al., 2015). The scores were graded according to three parameters: alveolar interval inflammation, inflammatory cell infiltration in bronchus, inflammatory cell infiltration in or surrounding the vasculature. Each parameter was scored as follows: 0 corresponded to no inflammation; 1 to occasional cuffing with inflammatory cells; 2 to moderate inflammatory cells and 3 to severe inflammatory cell infiltration. The total lung inflammation score was calculated by adding up the individual scores. Six sections from different guinea pigs in each group were scored. Masson's trichrome staining was used to visualize collagen deposition and fibrosis. The scores were based on the percentage of goblet cells and were calculated as follows: 0: none; 1: ≤ 25%; 2: 25 – 50%; 3: 50 – 75%; and 4: ≥ 75% goblet cells (Ma et al., 2016). Six sections from different guinea pigs in each group were examined and their scores were assessed by two experienced researchers, who were blinded to the information of samples.

2.5 Determination of cytokines and IgE level

The levels of interleukin 4 (IL-4), IL-5, IL-13 and IgE in the serum of guinea pigs were determined using the enzyme-linked immunosorbent assay (ELISA) kit from CUSABIO Biotech (Wuhan, China) according to the manufacturer's instructions. All tests were performed in duplicate. Optical densities were measured at 450nm by a microplate reader.

2.6 Quantitative reverse transcription polymerase chain reaction (RT-qPCR)

IL-4, IL-5, IL-13 and orosomucoid-like 3 (ORMDL3) mRNA levels in lung tissues were determined by RT-qPCR. Total lung RNA was extracted with TRIzols (Sigma-Aldrich, St Louis, MO, USA) and reverse-transcribed to cDNA according to the manufacturer's instructions (Takara, Dalian, China). RT-qPCR was performed on the cDNA samples according to the instructions of the SYBRs Premix Ex Tap™ II (Takara, Dalian, China). The reaction conditions were as follows: 95 °C for 30 s, followed by 45 cycles of denaturation at 95 °C for 5 s and 60 °C for 34 s. The used primers (Sangon

Biotech, Shanghai, China) were listed in Table 1. The expression level of each gene was normalized to endogenous GAPDH expression level, and reported as fold-change relative to normal control group.

2.7 Western blot analysis

Lung tissues from guinea pigs were lysed in RIPA buffer containing PMSF and phosphatase inhibitors (Nanjing Jiancheng Bioengineering Institute, Nanjing, China) followed by quick freezing. Proteins were extracted using a kit according to the manufacturer's protocol (Beyotime Biotech Inc, Nanjing, China) and the protein concentrations were measured using a bicinchoninic acid protein concentration assay kit. The proteins were separated by sodium dodecyl sulfate-polyacrylamide gel electrophoresis (SDS-PAGE) and transferred to polyvinylidene fluoride membranes (0.45 mm, Millipore, Boston, MA, USA). Non-specific sites were blocked with 5% bovine serum albumin (BSA) in tris-buffered saline containing 0.1% Tween 20 (TBST) for 2h and the blots were incubated with specific primary antibodies, including anti-p65 NF-κB, anti-phospho-p65 NF-κB, anti-IκB, anti-phospho-IκB and GAPDH proteins antibodies (1:1000, Cell Signaling Technology, Boston, MA, USA) for 12 h at 4℃. The membranes were rinsed 3 times with TBST for 5 min and incubated for 1 hour at a ratio of 1:1000 to secondary immunoglobulin conjugated horseradish peroxidase (Sigma-Aldrich, St. Louis, MO, USA) at 25℃. The membranes were then extensively washed with TBST, and detected by an enhanced chemiluminescence method (ECL kit, Millipore, USA). Image of blot immune-staining was captured and analyzed using Image J software to determine the phosphorylated to total protein ratio.

2.8 Chemical analysis of TWDS prescription

2.8.1. Extraction procedure

Accurately weighed 0.1g TWDS prescription powder samples were sonicated with 1mL methanol for 30 min. Then, the mixture was centrifuged at 14000 rpm at 4°C for 15 minutes. The solution was filtered through 0.45 μm membrane filters prior to chemical analysis.

2.8.2. Ultra performance liquid chromatography coupled with electrospray ionization orbitrap mass spectrometry (UPLC-ESI-Orbitrap-MS)

UPLC-ESI-Orbitrap-MS analysis was performed on Orbitrap Fusion Lumos Tribrid Mass Spectrometer (Thermo Fisher Scientific, U.S.A.) with UPLC (ACQUITY UPLC System, Waters, USA). An UPLC C18 analytical column (2.1 mm × 100 mm, I.D. 1.8μm, ACQUITY UPLC®HSS T3, Waters, U.S.A.) was used for separation at 40℃. The mobile phase was a mixture of water (A) and acetonitrile (B), both containing 0.1% (v/v) formic acid, with a linear gradient elution as follows: 0–1 min, 98% A; 1–5 min,

80% A; 5–13 min, 71% A; 13–17 min, 20% A, 17–18 min, 98% A, 18–20 min, 98% A. The injection volume was 3 μL. The flow rate was set at 0.30 mL/min.

Heated electrospray ionization was used in both positive and negative ion modes. The operation parameters were as follows: spray voltage static (positive ion 3600 V, negative ion 2300 V) sheath gas flow rate 20 units, auxiliary gas flow rate 10 units, sweep gas 10 units, ion transfer tube temperature 300°C, vaporizer temperature 200°C. The mass spectra were acquired in full scan mode from 100 to 1200 in mass to charge ratio (m/z) with a mass resolution of 120000, RF Lens 30%. The mass spectra were collected in centroid mode. Data were evaluated by Quan/Qual Browser and Xcalibur 4.0 (Thermo Fisher Scientific, U.S.A.)

2.9 Metabolomics

2.9.1 Quality control sample preparation method

An aliquot of 150 μL of each serum sample was pooled, vortexed and aliquoted to provide a quality control (QC) sample, and kept at -80 ℃ until use. QC samples went through the extraction protocols as described below as similar to all other samples. Before the start of chemical analysis, five repeated injections of the same QC sample were used to verify the working condition the instruments. Afterwards, the QC sample was injected to monitor the stability of the instruments after every five-sample run.

2.9.2 Sample preparation

100μL serum from each sample was mixed with 300μL cold methanol, which contained 5ppm of cholic acid D_4 as internal standard, and then vortexed for 30 s. The mixture was cooled in a freezer at -20℃ for one hour prior to centrifugation at 14000rpm under 4℃ for 15 min. 320μL supernatant was dried with nitrogen gas and reconstituted in 100μL 50% methanol in water followed by centrifugation at 14000rpm under 4℃ for 10 min. The supernatant was obtained for subsequent UPLC-ESI-QTOF-MS analysis.

2.9.3 Ultra-performance liquid chromatography combined with electrospray ionization quadrupole time-of-flight mass spectrometry (UPLC-ESI-QTOF-MS) condition

4μL aliquot was injected into a Waters ACQUITY UPLC system. The separation was performed on a Waters ACQUITY UPLC HSS T3 column (2.1 mm × 100 mm, 1.8 μm) with HSS T3 pre-column (2.1 mm × 5 mm, 1.8 μm, Waters Corporation, Milford, MA). The mobile phase consisted of combinations of A (0.1% formic acid in water, v/v) and B (0.1% formic acid in acetonitrile, v/v) at a flow rate of 0.3 ml/min with elution gradient as follows: 0-1min, 5% B; 5 min, 40% B; 8 min, 50% B; 16 min, 65% B; 17-20 min, 95% B. A 3-min post-run time was set to fully equilibrate the column. Column temperature and sample chamber temperature were 40℃ and 6℃ respectively.

MS was performed on a Waters SYNAPT G2 Q-IM-TOF HDMS system (Waters, Milford, USA) operating in an ESI in both positive and negative modes. Nitrogen was used as nebulization and cone gas. The nebulization gas was set to 550 L/h at a temperature of 400 ℃, and the cone gas was set to 40 L/h. The source temperature was set at 120 ℃. The capillary voltages in positive and negative ion modes were 3.0 kV and 2.2 kV, respectively. The sampling and extraction cone voltages were 40 V and 4.0 V, respectively. The data acquisition rate was set to 1 s with a 0.024 s interscan delay. Data between m/z 50 to 1000 were recorded in the centroid mode. For accurate mass acquisition, a lock-mass of leucine enkephalin at a concentration of 10 ng/mL was used via a lock spray interface at a flow rate of 5 uL/min, 3.0 eV trap collision energy, 2.2 kV capillary energy and 40 V cone voltage, monitoring for positive ion mode ($[M+H]^+$: 556.2771) and negative ion mode ($[M-H]^-$: 554.2615) to ensure accuracy during the MS analysis. MS/MS analysis was carried out to study the structure of potential biomarkers. In this section, argon was employed as collision gas and the collision energy was set between 20 and 50 eV according to the situation.

2.9.4 Data processing and analysis

The peak picking and alignment of all raw UPLC–MS data were conducted by Progenesis QI software (Nonlinear Dynamics, Newcastle upon Tyne, United Kingdom) in both ionization modes. Data were imported in the following setting prior to peak picking: resolution (full width at half maximum), 20000; retention time limit, 0.3-20 min; data type, centroided while other settings were set at default. All ion abundance was normalized by internal standard of its own sample to generate a data matrix that consisted of the retention time, m/z value, and the normalized ion abundance.

Quality screening was done by filtering out those metabolites whose relative standard deviation was greater than 30% in quality control samples to reduce the contribution of unstable peaks and eliminate noise from the dataset.

The resultant data matrices were introduced to Extended Statistical tool EZinfo v2.0 software (Umetrics AB, Sweden) for multivariate analysis. The data were scaled to unit variance for principal component analysis (PCA) to give an overview of the repeatability of QC samples. The QC samples with high repeatability should cluster together in the score plot of PCA. The samples excluding QC samples were pareto-scaled for partial least squares-discriminant analysis (PLS-DA) and orthogonal partial least squares - discriminant analysis (OPLS-DA). Potential markers of interest were extracted from the variable importance in the projection (VIP) values (threshold of VIP ≥ 1) and the location in S-loading plot of OPLS-DA based on their contribution to the

variation and correlation in the data set. The markers were identified by LC-MS/MS and matched with the METLIN (http://metlin.scripps.edu), the Mass Bank (http://www.massbank.jp/) and the Human Metabolome Databases (www.hmdb.ca) and/or confirmed by literatures and authentic standards based on retention times, mass fragmentation pattern and accurate masses (mass error <5 ppm).

2.10 Statistics

All data were shown as the mean ± standard deviation (SD), and one-way ANOVA was used to calculate significant differences between the groups. Statistical differences were considered significant if the P value was less than 0.05. All statistical analyses were performed using SPSS 19.0 (SPSS Inc., USA.).

3. Results

3.1 Chemical constituents of TWDS prescription

Quantitative analysis of ephedrine hydrochloride, sinapine thiocyanate, tetrahydropalmatine, baicalin and asarinin in raw herbal materials of Ephedra Herba, Sinapis Semen, Corydalis Rhizoma, Scutellariae Radix and Asari Radix et Rhizoma was carried out, respectively and all samples fulfilled the requirement stipulated in the 2015 Chinese Pharmacopoeia (supplementary document). In addition, 49 components, including organic acids, phenolic and its glycosides and alkaloids, were tentatively identified by UPLC-ESI-Orbitrap-MS after comparison of the accurate m/z and mass fragmentation pattern with literatures as well as online database. The base peak chromatogram of extract of TWDS prescription was depicted in Figure 1 and a summary of phytochemicals detected by UPLC-ESI-Orbitrap-MS was shown in Table 2.

3.2 Pathology of lung tissue inflammation

Histological analysis was performed on lung sections derived from guinea pigs and the results were presented in Figure 2. A huge number of inflammatory cells, including lymphocytes and eosinophilic granulocytes, were found in the alveolar septa around the bronchus in the OVA sensitization model group (Figure 2a), indicating that guinea pig asthma model had been successfully established. In addition, tissue damage and inflammation cells infiltration in bronchial and alveolar interval, bronchus, and the vasculature in the DSP and AST using TWDS treatment groups were significantly reduced compared with the OVA model group (Figure 2a).

Lung tissues with H&E staining revealed that an extensive hyperplasia and hypertrophy in goblet cells was visualized in the OVA group. The submucosa also showed evidence of infiltration of inflammatory cells together with smooth muscle thickening. A number

of inflammatory cells, including lymphocytes and eosinophilic granulocytes, were found in the alveolar septa around the bronchus in the OVA sensitization model group when compared with the normal control group. The inflammation score of the OVA group was 7.7 ± 1.21 while that score of the normal control group was 2.0 ± 0.89. Normal histological structure and minimal inflammation in the normal control group were clearly indicated (Figure 2b). After administration of DSP and AST, infiltration of inflammatory cells in lung tissue was reduced. Pulmonary hyperemia, edema phenomenon, the extent of bronchial wall and alveolar wall thickening were alleviated and the inflammation scores of DSP and AST treatment were 4.2 ± 1.17 and 4.7 ± 1.21, respectively ($p < 0.01$). The results indicated that airway fibrosis was significantly ameliorated after both administration of DSP and AST with TWDS.

3.3 Histological analysis performed on lung sections with Masson and H&E staining

Lung tissues with Masson staining among different groups for the assessment of collagen deposition were shown in Figure 2c. It was demonstrated that there was minimal collagen fibrosis in the normal control group, with a score of 0.50 ± 0.55. However, extensive collagen fibrosis in the airway was found in the OVA model group, with a score of 3.7 ± 0.52. In comparison with the OVA model group, the collagen deposition area around the airway and epithelium loss were reduced significantly in both the DSP (1.8 ± 0.75) and AST using TWDS (2.0 ± 0.89) treatment groups.

3.4 Effect of AST using TWDS treatment on IL-4, IL-5, IL-13 & total IgE in serum and IL-4, IL-5, IL-13 & ORMDL3 in lung tissue

Figure 3a and b summarized the effect of AST using TWDS treatment on IL-4, IL-5, IL-13 and total IgE in serum and lung tissue, respectively. The levels of IL-4, IL-5 and IL-13 in serum were increased significantly in the OVA model group compared with those in the normal control group ($P<0.01$). With the administration of DSP and AST using TWDS treatment for two weeks, the levels of IL-4, IL-5 and IL-13 in serum were significantly decreased in comparison with those of the OVA model group ($P < 0.01$ and $P < 0.05$). Similarly, both administration of DSP and treatment of AST using TWDS groups exhibited significantly inhibited levels of IgE when compared with those of the OVA model group ($P < 0.01$).

The results of RT-qPCR for determining the expression levels of various genes in lung tissues were shown in Figure 3c and d. There was a substantial increase in IL-4, IL-5 and IL-13 gene expression in the guinea pigs with OVA-induced asthma. Both administration of DSP and AST using TWDS treatment exhibited remarkable downregulation of IL-4, IL-5 and IL-13 mRNA expressions compared with the OVA model group. Similarly, the gene level of ORMDL3 was increased significantly in the

OVA-induced guinea pigs, while it was decreased distinctly after administration of DSP and AST using TWDS treatment in comparison with the OVA model group.

3.5 Effect of TWDS prescription acupoint application on NF-κB activation

NF-κB signaling is one of the recognized cytoprotective targets that mediates inflammation. Thus, the expression levels of proteins related to NF-κB pathway including p65 NF-κB (p65), phosphorylated-p65 NF-κB (p-p65), IκB and phosphorylated-IκB (p-IκB) were examined using Western blot analysis. As shown in Figure 4, the ratios of p-p65/p65 and p-IκB/IκB were significantly higher in the OVA model group compared with those in the normal control group ($p < 0.01$). However, the ratios of p-p65/p65 and p-IκB/IκB were significantly decreased in both administration of DSP ($p < 0.01$) and treatment of AST using TWDS groups ($p < 0.05$).

3.6 Stability of metabolomics platform

The stability of UPLC-ESI-QTOF-MS detection was assessed by multiple injections of the same pooled QC sample with a known concentration of an internal standard being added throughout the whole experimental run. Principle component analysis (PCA) score plot was used to evaluate the stability of the analytical instruments. Figure 5a showed the QC sample injections of inter-day experiments were clustered together in the PCA score plots. In addition, the coefficients of variation of internal standard were 10.2% and 8.0% in positive and negative ionization modes, respectively. Both results demonstrated that high reproducibility was achieved across the runs. This also ensured those changes among the different groups observed from the statistical analysis were related to the different interventions.

3.7 Effects on Metabolite changes

In the data collected from UPLC-MS, peak extraction by Progenesis QI obtained 3734 and 2875 peaks in all samples under positive and negative modes, respectively. After quality screening (QC's CV ≤ 30%), 2402 and 1955 metabolite features were detected at positive and negative modes, respectively.

Changes in metabolites in the blood serum were investigated by using OPLS-DA and Figure 5b showed clear separation between the normal control and the OVA model groups. Metabolites with significant contribution to the differentiation of the two groups by OPLS-DA were identified by their variable importance in the projection (VIP) values (threshold of VIP > 1) and the location in S-loading plot.

To reveal the underlying action of both administration of DSP and treatment of AST using TWDS, PLS-DA was applied and the results were depicted in Figure 5c. It was

clearly indicated that there was obvious separation among the normal control, OVA, DSP and AST using TWDS groups. 594 and 500 metabolites features detected at positive and negative modes, respectively were obtained and some highlighted potential metabolites were listed in Table 3. Their identities were tentatively confirmed by comparison with external standard, MS-MS data or online databases.

4. Discussion

Currently, corticosteroid drugs such as dexamethasone sodium phosphate (DSP) remain the first-line treatment for patients with chronic asthma. However, there are many side effects such as hyperglycemia, adrenal suppression and osteoporosis when high dosages are applied (Sarnes et al., 2011). In the present study, the beneficial effects of AST using TWDS on the skin tissue of guinea pigs were studied by using an ovalbumin-induced asthma model, which has been utilized extensively for modeling human asthma (Nials and Uddin, 2008). Ovalbumin served as the source of allergen in this work, and a Type 1 immune response was triggered after sensitization and aerosol challenge. A Th2-skewed response characterized by Th2 cytokines such as interleukin-4 (IL-4), IL-5, and IL-13 tends to mediate the production of ovalbumin-specific immunoglobulin type E (IgE) by B cells (Chini et al., 2014; Manson et al., 2009). It is one of the strong risk factors for developing asthma, in which IL-4 is important for allergic sensitization and IgE production; while IL-5 is crucial for eosinophil survival and IL-13 has pleiotropic effects in the lungs (Gilfillan and Tkaczyk, 2006; Finkelman et al., 2010).

Our experimental results were consistent with clinical observations that there were significant differences in the level of IL-4, IL-5, IL-13 and IgE between the OVA model group and the normal control group (Renauld, 2001). The reduction in serum level of IL-4, IL-5, IL-13 and IgE as a result of administration of DSP and treatment of AST using TWDS certainly played an important role in the therapeutic effects of these intervention.

Results of histopathological examination of the lung tissue using H&E also indicated that there was excessive infiltration of inflammatory cells, mostly eosinophils and lymphocytes, in the OVA model group compared with the normal control group. In addition, both administration of DSP and treatment of AST using TWDS could lower cell accumulation in the peribronchiolar, perivascular and alveolar regions and result in decrease in lung inflammation scores, compared with the OVA model group. Overexpression of Th2 cytokines and I gE is known to enhance collagen deposition in the lung tissue (Busse et al., 2001). Moreover, airway mucus was mainly secreted by airway goblet cells, and its proliferations contributed to the pathologic changes in airway remodeling and exacerbation of asthma (Rogers, 2007; Davis and Dickey, 2015).

Masson staining results showed that sub-epithelial collagen deposition (blue stain) arisen in the airway was significantly reduced in both the administration of DSP and treatment of AST using TWDS groups. This implied that treatment of AST using TWDS might be significant as a new anti-allergic agent for asthma management.

The allergic immune response of asthma is a complex process, and the pathophysiological responses, including lung eosinophilic inflammation, smooth muscle contraction and increased mucus production, result in airway obstruction and eventually lung damage (Bosnjak et al., 2011). From our metabolomics data, the level of leukotriene B4, which is a pro-inflammatory mediator produced from leukocytes, was significantly increased in the OVA model group compared with the normal control group. Other anti-inflammatory phospholipid metabolites such as lysoPC (18:0) and lysoPC(20:3) in the OVA model group were also significantly decreased, compared with the normal control group. However, with the administration of DSP and treatment of AST using TWDS, the level of leukotriene B4 was downregulated back to the normal control while the levels of lysoPC (18:0) and lysoPC (20:3) were upregulated back to the normal control. A similar trend was obtained in the fatty acid metabolism. Levels of anti-inflammatory metabolites such as C20:5 and C22:5 (DPA) in the OVA model were decreased significantly, compared with the normal control group. At the same time, both metabolites were upregulated to the normal level in the AST using TWDS treatment group.

Epinephrine, also known as adrenaline, is a naturally occurring metabolite in the human body and is used to relax the bronchial smooth muscle for the treatment of asthma. It has been reported that epinephrine levels in asthma patients do not increase as rapidly as needed to alleviate bronchoconstriction (Barnes et al., 1980; Aalderen van et al., 1991). Thus, it has been proposed that this weak increase in circulating epinephrine is an important factor in the pathogenesis of asthma (Bates et al., 1994). In this study, the measured level of epinephrine in the OVA model group was significantly higher than that of the normal control group, an observation that was consistent with previous literatures. With the treatment of AST using TWDS and administration of DSP, the level of epinephrine in serum of both groups was downregulated.

Xanthine is a key metabolite in purine metabolism and has been reported to have close relationship with neutrophilic inflammation of chronic obstructive pulmonary disease (Esther et al., 2015). Increased uric acid (end product of purine metabolism) levels of bronchoalveolar lavage fluids (BALF) in the airways of allergen-challenged asthmatic patients and mice were reported (Esther et al., 2015). In this study, the serum level of xanthine in the OVA model was decreased significantly compared with that of the

normal control group. Disturbance in purine metabolism due to asthma was observed and more xanthine might be converted into uric acid and secreted out in BALF. A recent study reported that the level of taurine, phenylalanine and xanthine in serum was decreased slightly in mild asthma patients (Reinke et al., 2017). With treatment of AST using TWDS, the level of xanthine in serum was upregulated to the level of the normal control group. It has been reported that xanthine could be used as a bronchodilator to treat asthma (Seddon et al., 2006). However, administration of DSP did not regulate it back to the normal level.

Spingolipid metabolites play an important role in the signaling events that influence cell behavior and functions and one of the sphingolipid metabolites, sphingosine-1-phosphate (S1P), influences the differentiation and responsiveness of mast cells, which are best known to trigger IgE-dependent / independent allergic diseases like asthma and chronic obstructive pulmonary disease (Saluja et al., 2015).S1P level in BALF has been found to be significantly increased from subjects with asthma compared with the normal control (Ammit et al., 2001). The biosynthesis of sphingolipids initiates in the endoplasmic reticulum where serine palmitoylransferase condenses serine and palmitoyl-CoA to generate 3-ketosphinganine, which is rapidly reduced to form sphinganine. Sphinganine is further converted into ceramides, which serve as a substrate for the production of sphingomyelins, gangliosides and sphingosine (Fyrst et al., 2010). S1P is derived from sphingosine through phosphorylation by two sphingosine kinases (SphK1 and SphK2), which are widely expressed in bronchial epithelium and airway smooth muscle cells while S1P can be irreversibly degraded by S1P lyase into ethanolamine phosphate and trans-2-hexadecenal (Fyrst et al., 2010). In this study, the levels of serine, sphinganine and ethanolamine phosphate in the OVA model were significantly decreased compared with those of the normal control group. Importantly, with treatment of AST using TWDS, the levels of serine, sphinganine and ethanolamine phosphate were upregulated back to the level of the normal control group. However, administration of DSP did not affect significantly this pathway.

OVA-induced allergic asthma caused serious disturbance to amino acid metabolism in our study. The levels of alanine and valine in the OVA group were upregulated and these trends are consistent with trends observed in previous literatures (Yu et al., 2016; Su et al., 2017). Treatment of AST using TWDS could downregulate these two amino acids back to the normal control level.

Odd chain phospholipids including LysoPC (17:0) and LysoPC (19:0) were uniquely detected in serum and both have been suggested to be bacterial in origin. With the treatment of AST using TWDS, the levels of these two metabolites were regulated back

to the normal level. However, our preliminary microbiota results found that there were no significant differences among all groups. In recent year, those odd phospholipid species have been found to be present in both plant and mammalian species (Rezanka and Sigler, 2009). They are also associated with some diseases such as cardiovascular and peroxisomal disorders due to α-oxidation (Jenkins et al., 2015).

Based on the findings deduced from non-target metabolomics, some follow-up works about the anti-inflammatory mechanism on lung tissue were carried out to elucidate the underlying signaling transduction pathway. NF-κB signaling pathway was proved to be closely associated with the development and progression of inflammation. Our results showed that the ratios of p-p65/p65 and p-IκB/IκB in the lung tissue were significantly reduced after treatment of AST using TWDS. For the reason above, the levels of cytokines including IL-4, IL-5, IL-13 and IgE in serum were close to those of the guinea pigs with DSP administration.

ORMDL3 and the associated 17q21 locus have been found as contributors of the genetic susceptibility and underlying pathogenesis of asthma through genome-wide association studies (Moffatt et al., 2007). The functions of ORMDL3 are not fully understood and it is known to be involved in sphingolipid metabolism and de novo sphingolipid synthesis. From our results obtained, the gene expression of ORMDL3 of lung tissue in OVA model group were also significantly increased, compared with the normal control group. However, with the administration of DSP and treatment of AST using TWDS, the level of gene expression of ORMDL3 was downregulated back to the normal control. It was clearly indicated that treatment of AST using TWDS could alter the sphingolipid metabolism.

Finally, the chemical constituents of TWDS used in this study were further explored by uplc-orbitrap-ms and a total of 50 chemical markers, including organic acids, phenolic and its glycosides and alkaloids, were tentatively identified. Many of these compounds have been reported to possess anti-inflammatory activity. For example, sinapic acid exerted anti-inflammatory effects in vivo by inhibiting NF-κB activation in macrophages, thereby inhibiting the production of iNOS, COX-2, and proinflammatory cytokines (Yun et al., 2008). Sesamin decreased OVA-induced secretion of IgE and cytokines, prevented eosinophil infiltration, and attenuated mucus oversecretion via the mechanism of decreasing phosphorylation levels of IκB-α and inhibiting NF-κB signaling pathways (Lin et al., 2014). Wogonin could alleviate airway inflammation through inhibition of STAT6 induced by Th2 cytokines in vivo (Ryu et al., 2015). Baicalein treatment reduced airway epithelial injury, ameliorated mitochondrial dysfunction and various features of airway inflammation in a mouse model of asthma

(Mabalirajan et al., 2013). Berberine exerted dose-dependent ameliorative effects on OVA-induced airway inflammation via the inhibition of the NF-κB signaling pathway in a rat model of asthma (Li et al., 2016). Thus, based on the chemical profiling of TWDS obtained, the pharmacological effects of TWDS may be a synergy of actions of multi-components. Further studies are needed to elucidate the lung-protective molecular mechanisms of TWDS in detail.

5. Conclusion

The present study confirmed that treatment of AST using TWDS had a markedly protective effect against OVA-induced allergic asthma in the guinea pig. This treatment not only attenuated airway inflammation and collagen deposition in the airway, but also decreased the levels of IL-4, IL-5, IL-13 and IgE in serum. In addition, metabolomics results showed that phospholipid, spingolipid, purine, amino acid metabolisms and the level of epinephrine were restored back to the normal level. Results of the gene expression of ORMDL3 in lung tissues indicated that AST using TWDS could alter the spingolipid metaboloism. Moreover, western blotting analysis demonstrated that its anti-asthmatic mechanism was via the inhibition of the NF-κB signaling pathway. Therefore, treatment of AST using TWDS could be a promising alternative for treating allergic asthma patients.

Author Contributions: S.J. Xiang and M.H. Li contributed equally to this work. S.J. Xiang, W.F. Wu, S.W. Cao, S.F. Ruan, Z.X. Wang and L.D. Weng performed the animal study, S.J. Xiang, Q. Shen, B.C. An, H.X. Zhu, and H.J. Chen performed the biological testing. M.H. Li performed the metabolomics work. M.H. Li, S.B. Chen, Y. Zhang and C.O Chan analyzed and interpreted the metabolomics data. A.C.Y. Yuen and H.H Tang performed the orbitrap mass spectrometer experiment. C.O Chan, S.J. Xiang and M.H. Li prepared the first draft of the manuscript. M.Y.M. Wong overviewed all mass spectrometer data. Q. Liu and D.K.W. Mok designed and supervised the whole study and reviewed the manuscript.

Conflicts of Interest: We declare no conflict of interest

6. Acknowledgements

This study was supported by the National Natural Science Foundation of China (81373975, 81303203, 81503222 and 81774329), the Hong Kong Chinese Material Medica Standards Project, the Shenzhen Basic Research Program (JCYJ20151030164008764, JCYJ20160229173844278, JCYJ20160330171116798, JCYJ20140819153305694), Natural Science Foundation of Shanghai (17ZR1430800), and Longhua Medical Innovation Team Program (LYCX-01). We are

also very grateful for the Large Equipment Funds and the University Research Facility in Chemical and Environmental Analysis of the Hong Kong Polytechnic University for providing the instruments used in this study. We sincerely thank Miss Josephine Leung for proofreading our manuscript.

7. Reference

Aalderen van, W.M., Postma, D.S., Koëter, G.H., Knol, K., 1991. Nocturnal airflow obstruction, histamine, and the autonomic central nervous system in children with allergic asthma. Thorax. 46, 366-371.

Ammit, A. J., Hastie, A. T., Edsall, L. C., Hoffman, R. K., Amrani, Y., Krymskaya, V. P., Kane, S. A., Peters, S. P., Penn, R. B., Spiegel, S., Panettieri, Jr., R. A., 2001. Sphingosine 1-phosphate modulates human airway smooth muscle cell functions that promote inflammation and airway remodeling in asthma. Faseb J. 15, 1212.

Barnes, P., FitzGerald, G., Brown, M., Dollery, C., 1980. Nocturnal asthma and changes in circulating epinephrine, histamine, and cortisol. N Engl J Med. 303, 263-267.

Bates, M.E., Clayton, M., Calhoun, W., Jarjour, N., Schrader, L., Geiger, K., Schultz, T., Sedgwick, J., Swenson, C., Busse W.,1994. Relationship of plasma epinephrine and circulating eosinophils to nocturnal asthma. Am J Respir Crit Care Med. 149, 667-672.

Bosnjak, B., Stelzmueller, B., Erb, K.J., Epstein, M.M., 2011. Treatment of allergic asthma: Modulation of Th2 cells and their responses. Respiratory Research. 12,114.

Busse, W.W., Lemanske, R.F. Jr., 2001. Asthma, N Engl J Med. 344, 350-362.

Chini, L., Monteferrario, E., Graziani, S., Moschese, V., 2014. Novel treatments of asthma and allergic diseases. Paediatr Respir Rev. 15, 355-362.

Davis, C. W., Dickey, B. F. 2015. Regulated airway goblet cell mucin secretion. Annual Review of Physiology. 70,487-512.

Delgadocharro, M.B., Guy, R.H. 2014. Effective use of transdermal drug delivery in children. Adv Drug Deliv Rev. 73,63-82.

Esther, C.R., Jr., Coakley, R.D., Henderson, A.G., Zhou, Y.H., Wright, F.A., Boucher, R.C., 2015. Metabolomic Evaluation of Neutrophilic Airway Inflammation in Cystic Fibrosis. Chest. 148, 507-515.

Finkelman, F.D., Hogan, S.P., Hershey, G.K.K., Rothenberg, M.E., Wills-Karp, M., 2010. Importance of Cytokines in Murine Allergic Airway Disease and Human Asthma. The Journal of Immunology. 184, 1663-1674.

Fyrst, H., Saba, J. D., 2010. An update on sphingosine-1-phosphate and other sphingolipid mediators. Nat Chem Biol. 6, 489-97.

Gilfillan, A.M., Tkaczyk, C., 2006. Integrated signalling pathways for mast-cell activation. Nature reviews. Immunology. 6, 218-230.

Gorrochategui, E., Jaumot, J., Lacorte, S., Tauler, R., 2016. Data analysis strategies for targeted and untargeted LC-MS metabolomic studies: Overview and workflow. TrAC Trends in Analytical Chemistry. 82, 425-442.

Jenkins, B., West, J.A., Koulman, A., 2015. A review of odd-chain fatty acid metabolism and the role of pentadecanoic Acid (c15:0) and heptadecanoic Acid (c17:0) in health and disease. Molecules. 20, 2425-2444.

Jiao, H.Y., Su, W.W., Li, P.B., Liao, Y., Zhou, Q., Zhu, N., He, L.L., 2015. Therapeutic effects of

699 naringin in a guinea pig model of ovalbumin-induced cough-variant asthma. Pulmonary
700 pharmacology & therapeutics. 33, 59-65.
701 Kool, M., Willart, M.A., van Nimwegen, M., Bergen, I., Pouliot, P., Virchow, J.C., Rogers, N.,
702 Osorio, F., Reis e Sousa, C., Hammad, H., Lambrecht, B.N., 2011. An unexpected role for uric acid
703 as an inducer of T helper 2 cell immunity to inhaled antigens and inflammatory mediator of allergic
704 asthma. Immunity. 34, 527-540.
705 Larché, M., Robinson, D.S., Kay, A.B., 2003. The role of T lymphocytes in the pathogenesis of
706 asthma. Journal of Allergy and Clinical Immunology. 111, 450-463.
707 Li, Z.H., Zheng, J., Zhang, N., Li, C.D., 2016. Berberine improves airway inflammation and inhibits
708 NF-κB signaling pathway in an ovalbumin-induced rat model of asthma. J Asthma. 53, 999-1005.
709 Lin, C.H., Shen, M.L., Zhou, N., Lee, C.C., Kao, S.T., Wu, D.C., 2014.Protective effects of the
710 polyphenol sesamin on allergen-induced T(H)2 responses and airway inflammation in mice, PLoS
711 One, 9 e96091.
712 Liu, L., Liu, T., Li, G., Wang, Q., Ng, T., 2003. Isolation and determination of p-
713 hydroxybenzoylcholine in traditional Chinese medicine Semen sinapis Albae. Analytical and
714 Bioanalytical Chemistry. 376, 854-858.
715 Lv, M.Y., Chen, J.Q., Gao, Y.Q., Sun, J.Q., Zhang, Q.Q., Zhang, M.H., Xu, F.G., Zhang, Z.J., 2015.
716 Metabolomics based on liquid chromatography with mass spectrometry reveals the chemical
717 difference in the stems and roots derived from Ephedra sinica, J Sep Sci. 38, 3331-3336.
718 Ma, Y., Ge, A., Zhu, W., Liu, Y.N., Ji, N.F., Zha, W.J., Zhang, J.X., Zeng, X.N., Huang, M., 2016.
719 Morin Attenuates Ovalbumin-Induced Airway Inflammation by Modulating Oxidative Stress-
720 Responsive MAPK Signaling. Oxidative medicine and cellular longevity. 2016, 5843672.
721 Mabalirajan, U., Ahmad, T., Rehman, R., Leishangthem, G.D., Dinda, A.K., Agrawal, A., Ghosh,
722 B., Sharma, S.K., 2013. Baicalein reduces airway injury in allergen and IL-13 induced airway
723 inflammation. PloS one 8, e62916.
724 Manson, S.C., Brown, R.E., Cerulli, A., Vidaurre, C.F., 2009. The cumulative burden of oral
725 corticosteroid side effects and the economic implications of steroid use. Respiratory medicine. 103,
726 975-994.
727 Moffatt, M. F., Kabesch, M., Liang, L., Dixon, A. L., Strachan, D., Heath, S., Depner, M., von
728 Berg, A., Bufe, A., Rietschel, E., Heinzmann, A., Simma, B., Frischer, T., Willis Owen, S.A., Wong,
729 K.C., Illig, T., Vogelberg, C., Weiland, S.K., von Mutius, E., Abecasis, G.R., Farrall, M., Gut,
730 I.G., Lathrop, G.M., Cookson, W.O., 2007. Genetic variants regulating ormdl3 expression
731 contribute to the risk of childhood asthma. Nature. 448, 470-473.
732 Morin, C., Fortin, S., Cantin, A.M., Rousseau, E., 2011. Docosahexaenoic acid derivative prevents
733 inflammation and hyperreactivity in lung: implication of PKC-Potentiated inhibitory protein for
734 heterotrimeric myosin light chain phosphatase of 17 kD in asthma. American journal of respiratory
735 cell and molecular biology. 45, 366-375.
736 Morin, C., Fortin, S., Cantin, A.M., Rousseau, E., 2013. MAG-EPA resolves lung inflammation in
737 an allergic model of asthma. Clinical and experimental allergy : journal of the British Society for
738 Allergy and Clinical Immunology. 43, 1071-1082.
739 Nagana Gowda, G.A., Raftery, D., 2017. Recent Advances in NMR-Based Metabolomics. Anal.
740 Chem. 89, 490-510.
741 Nials, A.T., Uddin, S. 2008. Mouse models of allergic asthma: acute and chronic allergen challenge.
742 Dis Model Mech. 1,213.

743 Pavord, I.D., Beasley, R., Agusti, A., Anderson, G.P., Bel, E., Brusselle, G., Cullinan, P., Custovic,
744 A., Ducharme, F.M., Fahy, J.V., Frey, U., Gibson, P., Heaney, L.G., Holt, P.G., Humbert, M., Lloyd,
745 C.M., Marks, G., Martinez, F.D., Sly, P.D., Mutius von, E., Wenzel, S., Zar, H.J., Bush, A, 2017.
746 After asthma: redefining airways diseases. Lancet. https://doi.org/10.1016/S0140-
747 6736(17)30879-6.
748 Peng,J., Wu, X.Q., He,L.Y., Fang,y.g., Zi, M.J., Yan, S.Y., Liu,B.Y. 2012. Effects of summer
749 acupoint application therapy in reducing exacerbation frequency of chronic lung diseases: protocol
750 of a retrospective and prospective study, Journal of Chinese Integrative Medicine. 10,39-47.
751 Qiao, X., Li, R., Song, W., Miao, W.-j., Liu, J., Chen, H.-b., Guo, D.-a., Ye, M., 2016. A targeted
752 strategy to analyze untargeted mass spectral data: Rapid chemical profiling of Scutellaria baicalensis
753 using ultra-high performance liquid chromatography coupled with hybrid quadrupole orbitrap mass
754 spectrometry and key ion filtering. Journal of Chromatography A. 1441, 83-95.
755 Reinke, S.N., Gallart-Ayala H., Gómez, C., Checa, A., Fauland, A., Naz, S., Kamleh, M.A.,
756 Djukanović, R., Hinks, T.S., Wheelock, C.E.,2017. Metabolomics analysis identifies different
757 metabotypes of asthma severity. Eur Respir J. 49, 1601740.
758 Renauld, J.C. 2001. New insights into the role of cytokines in asthma. J Clin Pathol. 54,577-89.
759 Rezanka, T., Sigler, K., 2009. Odd-numbered very-long-chain fatty acids from the microbial, animal
760 and plant kingdoms. Progress in lipid research. 48, 206-238.
761 Rogers, D. F. 2007. Physiology of airway mucus secretion and pathophysiology of hypersecretion.
762 Respiratory Care. 52,1134.
763 Ryu, E.K., Kim, T.H., Jang, E.J., Choi, Y.S., Kim, S.T., Hahm, K.B., Lee, H.J., 2015.Wogonin, a
764 plant flavone from Scutellariae radix, attenuated ovalbumin-induced airway inflammation in mouse
765 model of asthma via the suppression of IL-4/STAT6 signaling. J Clin Biochem Nutr. 57,105-112.
766 Sagar, S., Akbarshahi, H., Uller, L., 2015. Translational value of animal models of asthma:
767 Challenges and promises. European Journal of Pharmacology. 759, 272-277.
768 Saluja, R., Kumar, A., Jain, M., Goel, S. K., & Jain, A., 2017. Role of sphingosine-1-phosphate in
769 mast cell functions and asthma and its regulation by non-coding rna. Frontiers in
770 Immunology. https://doi.org/10.3389/fimmu.2017.00587.
771 Sarnes, E., Crofford, L., Watson, M., Dennis G, Kan H, Bass D, 2011. Incidence and US costs of
772 corticosteroid-associated adverse events: a systematic literature review. Clin Ther. 33, 1413-32.
773 Seddon, P., Bara, A., Lasserson, T. J., Ducharme, F. M., 2006. Oral xanthines as maintenance
774 treatment for asthma in children. Cochrane Database of Systematic Reviews. 1, CD002885.
775 Shu, X., Jiang, X.W., Cheng, B.C., Ma, S.C., Chen, G.Y., Yu, Z.L., 2016. Ultra-performance liquid
776 chromatography-quadrupole/time-of-flight mass spectrometry analysis of the impact of processing
777 on toxic components of Kansui Radix. BMC complementary and alternative medicine. 16, 73.
778 Su, L., Shi, L., Liu, J., Huang, L.F., Huang, Y., Nie, X.M.,2017. Metabolic profiling of asthma in
779 mice and the interventional effects of SPA using liquid chromatography and Q-TOF mass
780 spectrometry, Mol. BioSyst. 13, 1172-1181.
781 Wen, H., Gao, H.-y., Qi, W., Xiao, F., Wang, L.-l., Wang, D., Yuan, D., 2014. Simultaneous
782 Determination of Twenty-Two Components in Asari Radix et Rhizoma by Ultra Performance Liquid
783 Chromatography Coupled with Quadrupole Time-of-Flight Mass Spectrometry. Planta Medica. 80,
784 1753-1762.
785 Wu, C.-Y., Kong, M., Zhang, W., Long, F., Zhou, J., Zhou, S.-S., Xu, J.-D., Xu, J., Li, S.-L., 2018.
786 Impact of sulphur fumigation on the chemistry of ginger. Food Chemistry. 239, 953-963.

Xiang, S.J., Chen, H.J., Zuo, T., Hong, J.H., Cao, S.W., Ruan, S.F., Weng, L.D., Zhu, H.X., Liu, Q., 2016. Effect of 'Treating Winter Disease in Summer' Prescription on Skin Immune Barrier and Systemic Immunity in a Guinea Pig Model of Asthma. Int J Clin Dermatol Res. 4, 81-86.

Yu, M., Cui, F.X., Jia, H.M., Zhou, C., Yang, Y., Zhang, H.W., Ding, G., Zou, Z.M., 2016. Aberrant purine metabolism in allergic asthma revealed by plasma metabolomics. Journal of pharmaceutical and biomedical analysis. 120, 181-189.

Yun, K.J., Koh, D.J., Kim, S.H., Park, S.J., Ryu, J.H., Kim, D.G., Lee, J.Y., Lee, K.T., 2008. Anti-inflammatory effects of sinapic acid through the suppression of inducible nitric oxide synthase, cyclooxygase-2, and proinflammatory cytokines expressions via nuclear factor-kappaB inactivation, J Agric Food Chem. 56 10265-10272.

Zhang, L., 1990. Zhang shi yi tong. Shanghai Science Technology Publications, Shanghai.

Zhang, Z., Huang, Y., Tao, J., Li, Z., 2006. Internal Medicine of Traditional Chinese Medicine. Publishing house of shanghai university of traditional Chinese medicine, Shanghai

Zheng, X.J., Zheng, W.L., Zhou, J.J., Gao, X., Liu, Z.H., Han, N., Yin, J. Study on the discrimination between Corydalis Rhizoma and its adulterants based on HPLC-DAD-Q-TOF-MS associated with chemometric analysis, Journal of Chromatography B. DOI: 10.1016/j.jchromb.2017.10.028.

Zhong, J., Chen Y.F., Xie, W.J., Chen, L.J. 2009. Clinical Study about Curative Effect of the Crude Herb Moxibustion Ointment, Asia-Pacific Traditional Medicine. 5, 36-37.

807 Table 1: The sequence of primes for RT-qPCR analysis

Gene	Forward prime(5′-3′)	Reverse prime(5′-3′)
IL-4	GGAGAAGAGTCCCTGTGCCG	CGGAGGTAGGCTGTATGGTGC
IL-5	GCAGTTGGGTTTGCTGGCTCT	TCGCTCCTCCCCGCATTT
IL-13	CCGTGGTCCTTGCTCTTGC	GGTCTTCTGATCCTGGGTGATG
ORMDL3	CAGCGAGGTGAACCCTAACA	CTGAGGCAACTTGGGAATGA
GAPDH	AAGGTCGGAGTGAACGGATTT	TGGGGCTAAGCAGTTGGTG

808

Table 2: Compounds identified in TWDS prescription by UPLC-ESI-Orbitrap-MS

No.	Retention time	Molecular formula	$[M+H]^+$(m/z) (mass accuracy)(ppm)	$[M-H]^-$(m/z) (mass accuracy)(ppm)	Identification	Origins
1	3.27	$C_9H_{13}NO$	152.1065 (3.29)		Nor(pseudo)ephedrine	Ephedra sinica (Lv et al., 2015)
2	3.86	$C_{10}H_{15}NO$	166.1221 (3.01)		(pseudo)ephedrine	Ephedra sinica (Lv et al., 2015)
3	4.07	$C_{28}H_{36}N_4O_4$	493.2795 (2.84)		Ephedradine A	Ephedra sinica (Lv et al., 2015)
4	4.17	$C_{11}H_{17}NO$	180.1376 (3.89)		Methyl(pseudo)ephedrine	Ephedra sinica (Lv et al., 2015)
5	4.64	$C_{15}H_{14}O_6$	291.0854 (3.09)		Catechin	Ephedra sinica (Lv et al., 2015)
6	4.71	$C_8H_{12}N_2$	137.1069 (2.92)		Tetramethylpyrazine	Ephedra sinica (Lv et al., 2015)
7	5.16	$C_{10}H_{10}O_4$	195.0646 (3.08)		Kakuol	Asarum sieboldii (Wen et al., 2014)
8	6.05	$C_{15}H_{12}O_7$		303.0509(0.33)	(2R,3R)-3,5,7,2',6-Pentahydroxyglavanone	Scutellaria Baicalensis (Qiao et al., 2016)
9	6.61	$C_{26}H_{28}O_{13}$		547.1457(-3.84)	Chrysin 6-C-pen-8-C-hex	Scutellaria Baicalensis (Qiao et al., 2016)
10	6.74	$C_{54}H_{20}O_{12}$		463.0887(-1.08)	Carthamidin 7-O-glucuronide	Scutellaria Baicalensis (Qiao et al., 2016)
11	6.86	$C_{29}H_{36}O_{15}$		623.2003(-3.53)	Acteoside	Scutellaria Baicalensis (Qiao et al., 2016)
12	6.89	$C_{11}H_{12}O_5$	225.0757(3.11)		Sinapic acid	Semen Sinapis (Liu et al., 2003)
13	6.99	$C_{23}H_{24}O_{13}$		507.1145(-0.2)	Viscidlin III 6'-O-β-D-glucoside	Scutellaria Baicalensis (Qiao et al., 2016)
14	7.12	$C_{20}H_{23}NO_4$	342.17(3.51)		Corypalmine	Rhizoma Corydalis (Zheng et al., 2017)
15	7.30	$C_{29}H_{38}N_4O_5$	523.2933 (-3.44)		Ephedradine B/D	Ephedra sinica (Lv et al., 2015)
16	7.36	$C_{21}H_{25}NO_4$	356.1845(0.00)		Glaucine	Rhizoma Corydalis (Zheng et al., 2017)
17	7.46	$C21_1H_{20}O_9$		415.1032(0.72)	Chrysin-8-C-glucoside	Scutellaria Baicalensis (Qiao et al., 2016)
18	7.48	$C_{29}H_{36}O_{15}$		623.1981(0)	Acteoside isomer	Scutellaria Baicalensis (Qiao et al., 2016)
19	7.89	$C_{20}H_{19}NO_5$	354.1336(3.67)		Protopine	Rhizoma Corydalis (Zheng et al., 2017)

20	8.15	$C_{21}H_{20}O_9$		415.1033(0.48)	Chrysin 6-C-glucoside	Scutellaria Baicalensis (Qiao et al., 2016)
21	8.50	$C_{20}H_{20}O_6$	357.1333(3.64)		Pluviatilol	Asarum sieboldii (Wen et al., 2014)
22	8.52	$C_{20}H_{18}O_6$		353.1031(1.42)	Asarinin	Asarum sieboldii (Wen et al., 2014)
23	8.76	$C_{21}H_{23}NO_5$	370.1649(3.51)		Allocryptopins	Rhizoma Corydalis (Zheng et al., 2017)
24	8.91	$C_{21}H_{25}NO_4$	356.1856(3.09)		Tetrahydropalmatine	Rhizoma Corydalis (Zheng et al., 2017)
25	9.17	$C_{16}H_{14}O_6$		301.0714(1)	Trihydroxy-methoxyflavanone	Scutellaria Baicalensis (Qiao et al., 2016)
26	9.21	$C_{19}H_{14}NO_4$	320.0907(3.12)		Coptisine	Rhizoma Corydalis (Zheng et al., 2017)
27	9.87	$C_{21}H_{19}NO_4$	240.1533 (2.94)		Tetrahydroberberine	Rhizoma Corydalis (Zheng et al., 2017)
28	10.20	$C_{22}H_{27}NO_4$	370.2000(3.24)		Corydaline	Rhizoma Corydalis (Zheng et al., 2017)
29	10.33	$C_{21}H_{22}NO_4$	352.1532(0.57)		Palmatine / Dehydrocorybulbine	Rhizoma Corydalis (Zheng et al., 2017)
30	10.84	$C_{31}H_{40}O_{15}$		651.2308(-2.15)	Cistanoside D isomer	Scutellaria Baicalensis (Qiao et al., 2016)
31	10.89	$C_{21}H_{20}O_{11}$		447.0933(-1.79)	5,7,2’,6’-Tetrahydroxyflavone 2’-O-β-d-glucoside	Scutellaria Baicalensis (Qiao et al., 2016)
32	11.29	$C_{21}H_{18}O_{11}$		445.0776(-3.37)	Baicalein 7-glucuronide	Scutellaria Baicalensis (Qiao et al., 2016)
33	11.41	$C_{21}H_{22}NO_4$	352.1532(0.57)		Palmatine / Dehydrocorybulbine	Rhizoma Corydalis (Zheng et al., 2017)
34	11.58	$C_{20}H_{18}NO_4$	336.1218(3.57)		Berberine	Rhizoma Corydalis (Zheng et al., 2017)
35	11.73	$C_{22}H_{20}O_{12}$		475.0883(-0.21)	Trihydroxy-methoxyflavanone O-gluA	Scutellaria Baicalensis (Qiao et al., 2016)
36	12.27	$C_{22}H_{22}O_{11}$		459.0948(-3.27)	Baicalein O-gluA methyl ester	Scutellaria Baicalensis (Qiao et al., 2016)
37	12.45	$C_{22}H_{20}O_{12}$		475.0881(0.21)	Trihydroxy-methoxyflavanone O-gluA	Scutellaria Baicalensis (Qiao et al., 2016)
38	12.64	$C_{22}H_{24}NO_4$	366.1687(4.92)		Dehydrocorydaline	Rhizoma Corydalis (Zheng et al., 2017)
39	13.14	$C_{22}H_{22}O_{11}$		459.0948(-3.27)	Wogonoside	Scutellaria Baicalensis (Qiao et al., 2016)
40	13.71	$C_{23}H_{22}O_{12}$		489.1039(-0.2)	5,7-Dihydroxy-8,2'-dimethoxyflavone	Scutellaria Baicalensis (Qiao et al., 2016)
41	14.05	$C_{23}H_{24}O_{12}$		491.1192(0.61)	5,2',6'-Dihydroxy-7,8-dimethoxyflavone 412'-O-β-D-glucoside	Scutellaria Baicalensis (Qiao et al., 2016)

42	14.81	$C_{16}H_{12}O_6$		299.0559(0.67)	Trihydroxy-methoxyflavone	Scutellaria Baicalensis (Qiao et al., 2016)
43	15.16	$C_{15}H_{10}O_5$		269.0455(-2.23)	Baicalein	Scutellaria Baicalensis (Qiao et al., 2016)
44	16.23	$C_{16}H_{12}O_5$		283.0619(2.47)	Wogonin	Scutellaria Baicalensis (Qiao et al., 2016)
45	16.23	$C_{15}H_{10}O_4$		253.0513(2.77)	Chrysin	Scutellaria Baicalensis (Qiao et al., 2016)
46	16.52	$C_{17}H_{26}O_4$		293.1758(-0.68)	6-gingerol	Zingiber officinale (Wu et al., 2018)
47	17.04	$C_{21}H_{34}O_4$	351.253(3.7)		10-gingerol	Zingiber officinale (Wu et al., 2018)
48	17.74	$C_{41}H_{47}O_{15}$	794.3018(3.78)		Kansuinine D	Euphorbia Kansui (Shu et al., 2016)
49	17.75	$C_{17}H_{24}O_4$	293.1747(3.75)		6-dehydro-6-gingerol	Zingiber officinale (Wu et al., 2018)

*Marker confirmed by comparing the database and literatures (Lv et al., 2015; Shu et al., 2016; Qiao et al., 2016; Wen et al., 2014; Zheng et al., 2017; Wu et al., 2018; Liu et al., 2003)

Table 3: Trend of changes in metabolites identified by UPLC-ESI-QTOF-MS

Metabolites	Retention time (min)	^Adducts	Theoretical m/z	Detected m/z	Mass error (ppm)	Fold Change			*p* value of one-way ANOVA compared to Model group			VIP value of OPLS-DA
						Model / Control	DSP / Control	AST / Control	Control	DSP	AST	
Epinephrine#	0.89	$[M+H]^+$	184.0968	184.0969	-7.06	1.95	0.45	0.62	0.008	0.097	0.042	1.58
Valine#	0.89	$[M+H]^+$	118.0863	118.0867	3.39	0.46	0.85	1.00	0.024	0.195	0.032	1.33
Norepinephine	0.93	$[M-H_2O+H]^+$	152.0706	152.0687	-12.5	1.68	1.85	1.58	0.32	0.979	0.993	1.39
Xanthine#	2.11	$[M+H]^+$	153.0407	153.0410	1.96	0.33	0.16	0.99	0.012	0.818	0.009	1.97
Androstenedione#	6.21	$[M+H]^+$	287.2006	287.2008	0.70	2.95	2.40	3.33	0.022	0.86	0.908	1.49
HEPE#	11.36	$[M-H_2O+H]^+$	301.2168	301.2163	-1.66	8.02	2.01	2.37	0.001	0.008	0.006	2.08
Stearidonic Acid#	14.29	$[M+H]^+$	277.2162	277.2166	1.44	2.76	0.43	0.70	0.042	0.013	0.011	1.24
LysoPC (20:3)#	14.57	$[M+H]^+$	546.3554	546.3557	0.55	0.44	0.95	1.13	0.044	0.68	0.012	1.12
Sphinganine#	15.22	$[M-H_2O+H]^+$	284.2948	284.2947	-0.35	0.27	0.37	0.96	0.029	0.982	0.031	1.67
LysoPC (17:0)#	16.20	$[M+H]^+$	510.3554	510.3561	1.37	0.28	0.79	1.16	0.03	0.161	0.008	1.18
LysoPC (20:2)#	16.47	$[M+H]^+$	548.3711	548.3712	0.18	0.22	0.66	1.55	0.02	0.327	<0.001	1.69
HETE#	17.62	$[M+Na]^+$	343.2244	343.2246	0.58	0.41	0.50	0.89	0.003	0.992	0.019	1.1
LysoPC (18:0)#	17.69	$[M+H]^+$	524.3711	524.3713	0.38	0.47	0.91	1.28	0.047	0.152	0.002	1.19
Leukotriene B4#	17.78	$[M-H_2O+H]^+$	319.2268	319.2245	-7.20	2.53	0.74	0.89	0.015	0.005	0.009	1.89
LysoPC (20:1)#	18.00	$[M+H]^+$	550.3867	550.3869	0.36	0.42	0.73	1.08	0.02	0.424	0.012	1.74
LysoPC (19:0)#	18.67	$[M+H]^+$	538.3867	538.3873	1.11	0.30	0.51	1.23	0.004	0.371	0.001	1.97

Serine #	0.82	$[M-H]^-$	104.0353	104.0352	-0.96	0.46	0.67	0.86	0.004	0.456	0.047	1.27
Alanine #	0.89	$[M-H]^-$	88.0404	88.0401	-3.41	2.64	2.35	1.02	<0.001	0.863	0.001	1.77
Xanthine #	2.11	$[M-H]^-$	151.0261	151.0249	-7.95	0.25	0.38	1.01	0.029	0.967	0.028	1.30
Glycocholic acid #	7.22	$[M-H]^-$	464.3018	464.301	-1.72	4.98	2.71	1.75	0.023	0.283	0.041	1.25
Phosphoethanolamine#	15.22	$[M-H]^-$	140.0118	140.0106	-8.57	0.36	0.64	1.07	0.022	0.575	0.007	1.10
Eicosapentaenoic acid#	16.32	$[M-H]^-$	301.2173	301.2163	-3.32	0.40	0.33	1.01	0.017	0.982	0.011	1.29
LysoPC20:2 #	16.49	$[M+FA-H]^-$	592.3620	592.3614	-1.01	0.23	0.77	1.03	0.038	0.069	0.032	1.32
LysoPC16:0#	17.61	$[M-CH_3]^-$	480.3096	480.3092	-0.83	0.45	0.85	1.48	0.034	0.243	<0.001	2.11
HETE#	17.64	$[M-H]^-$	319.2279	319.2271	-2.51	0.35	0.37	1.03	0.016	0.982	0.002	1.05
C22:5 #	17.9	$[M-H]^-$	329.2486	329.2481	-1.52	0.28	0.21	0.98	0.034	0.992	0.030	1.31
LysoPC20:1*	18	C20:1	309.2799	309.2799	0.00	0.52	0.80	1.41	0.004	0.213	0.021	1.10

One-way (ANOVA): *Tamhane's T2; #Tukey HSD post-hoc test.

Figure 1: The base peak chromatogram (BPC) of the methanol extract of by UPLC-orbitrap-ESI-MS in the positive (a) and negative (b) ion modes.

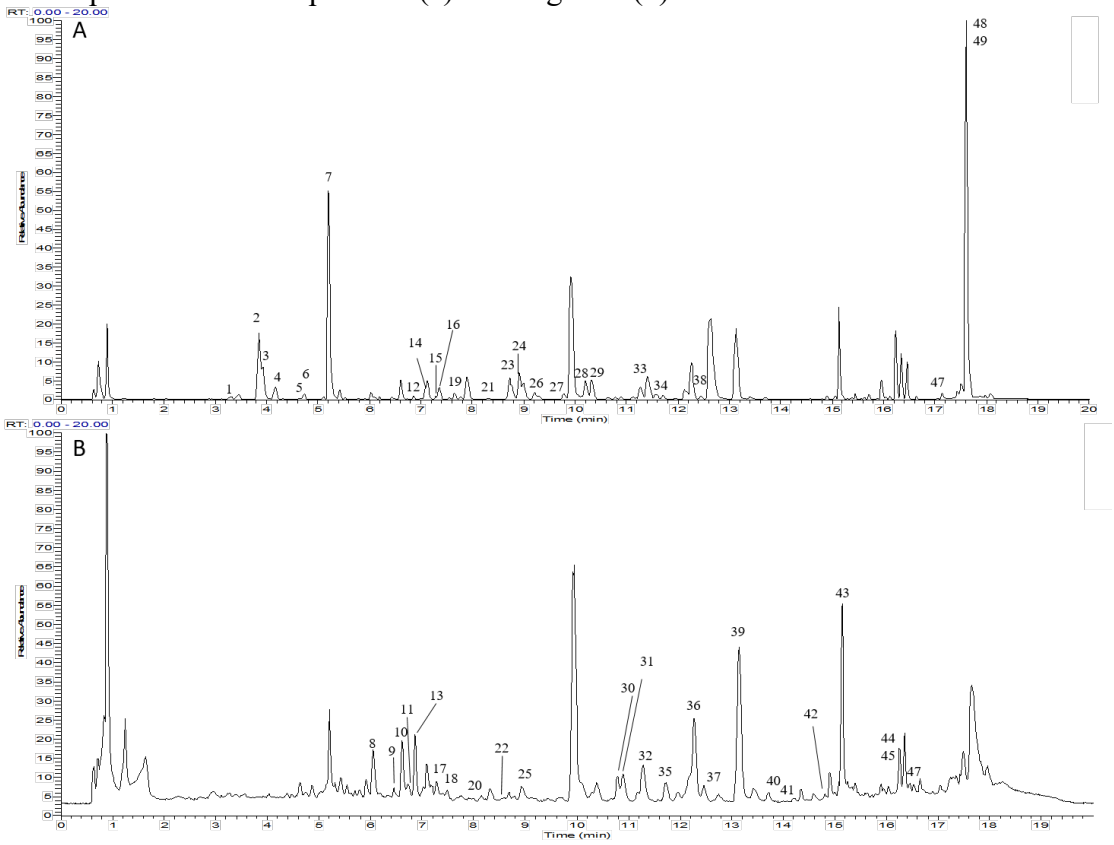

Figure 2: (a) H&E and Masson's trichrome staining of lung sections of guinea pigs with magnification (200×); (b) Histological semi-quantitative scores of lung inflammation; (c) Histological semi-quantitative scores of collagen deposition.
Each bar represents the mean ± SEM (n= 5-6). $^{\#}P<0.05$ and $^{\#\#}P<0.01$ vs the normal control group. *P<0.05 and **p<0.01 vs OVA group.

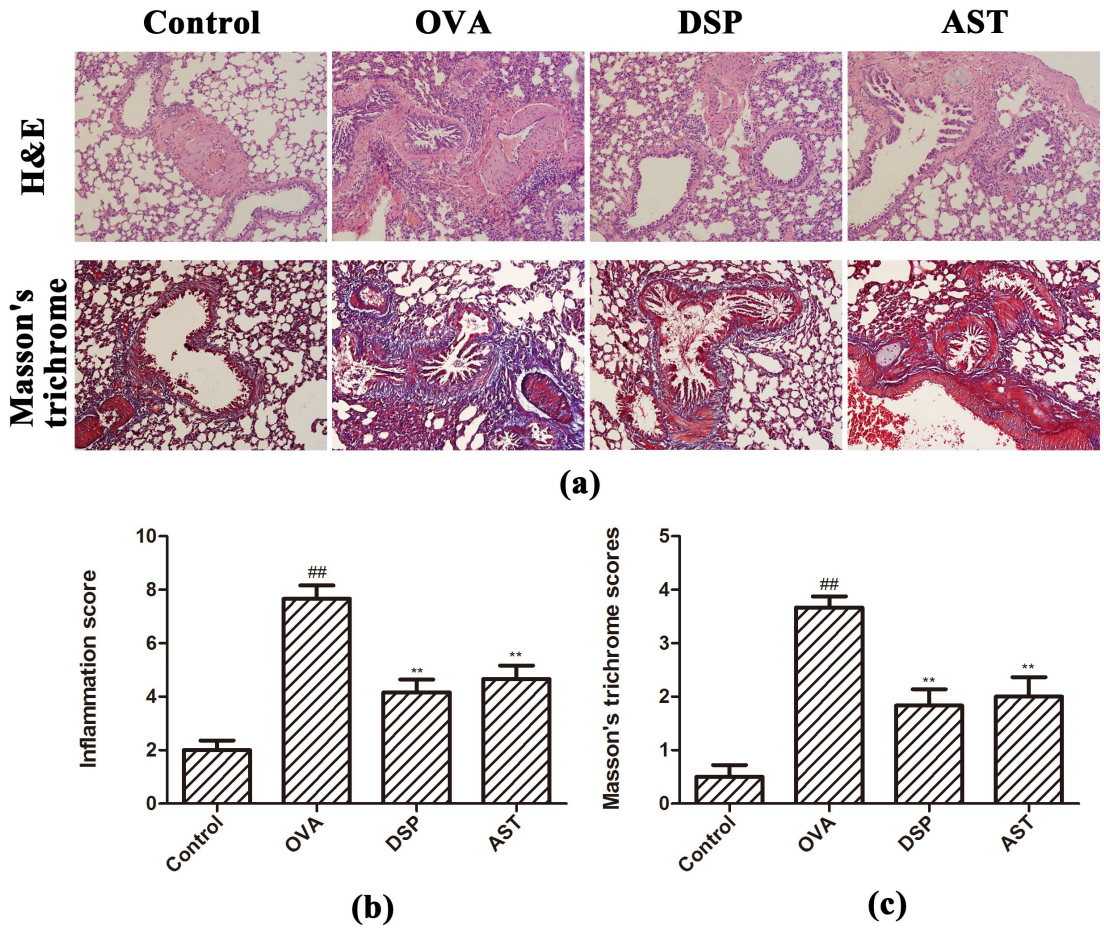

Figure 3: (a) Levels of cytokines of IL-4, IL-5, IL-13 in serum; (b) Levels of IgE in different groups of serum; (c) gene levels of IL-4, IL-5 and IL-13 in lung tissue; (d) gene levels of ORMDL3 in lung tissue (n=6).
Compared with the normal control group, $^{\#}P < 0.05$ and $^{\#\#}P < 0.01$; compared with the normal control group, $*P < 0.05$ and $**P < 0.01$ vs OVA model group.

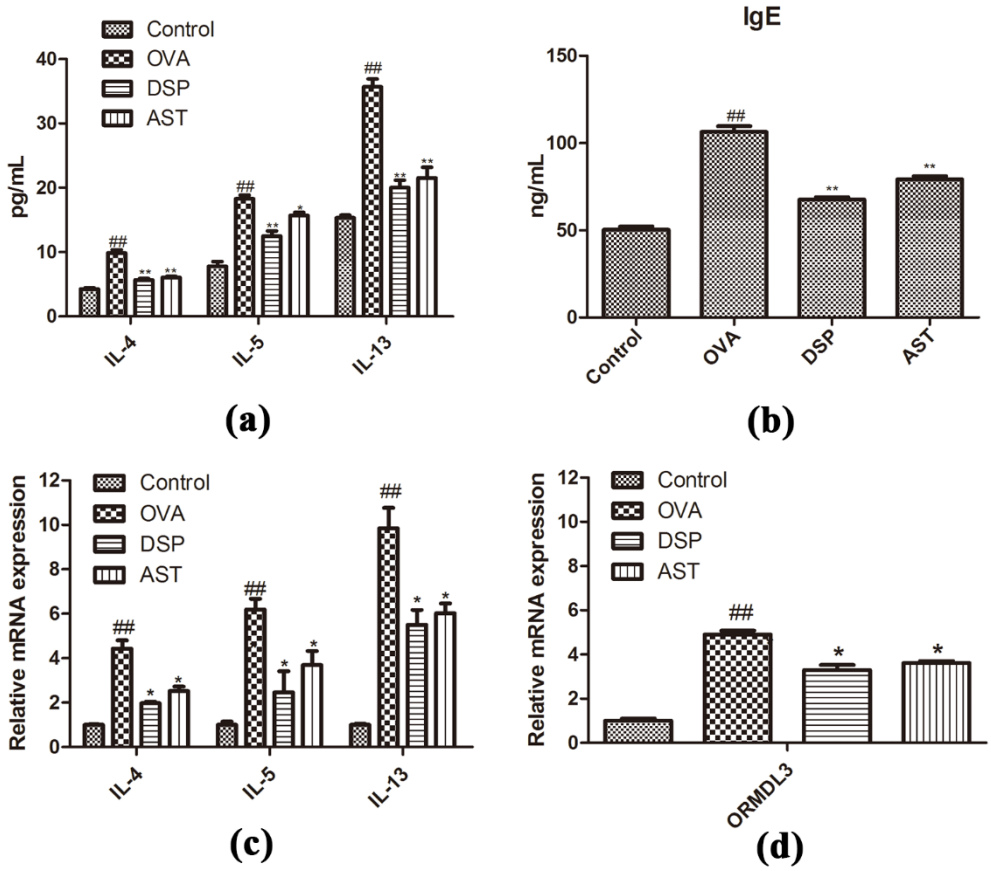

Figure 4: Protein levels of p65 NF-κB, p-p65 NF-κB, IκB, p-IκB in lung tissue. (a) Typical Western blot; (b) Semi-quantitative analysis of lung homogenate western blotting.
Compared with the normal control group, $^{\#}P < 0.05$ and $^{\#\#}P < 0.01$; compared with the normal control group, $^{*}P < 0.05$ and $^{**}P < 0.01$ vs OVA model group.

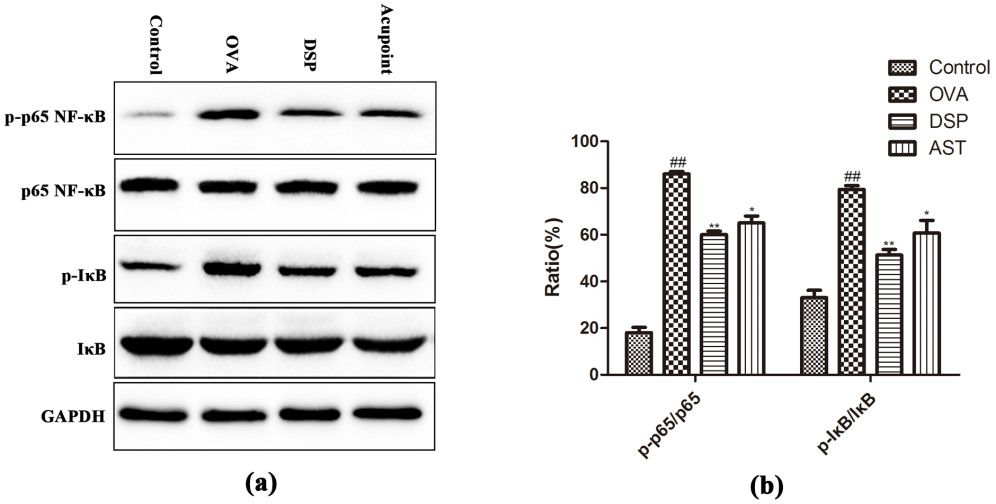

Figure 5: Results of metabolomics study
(a) PCA score plot (i) +ESI mode, (ii) –ESI mode (▲ AST using TWDS group), (● DSP group), (▼ OVA model group), (■ control group) and (* QC);
(b) (i) OPLS-DA score plot and (ii) S-plots of serum samples collected from the normal control and the OVA model groups based on UPLC-QTOF-MS acquired in positive ionization mode [$R^2X = 0.327$, $R^2Y = 0.983$, $Q^2 = 0.746$] (iii) OPLS-DA score plot and (iv) S-plots of serum samples collected from the normal control and the OVA model groups based on UPLC-qTOF-MS acquired in negative ionization mode [$R^2X = 0.416$, $R^2Y = 0.976$, $Q^2 = 0.770$], Red squares highlighted in (ii) were variable with VIP >1.5;
(c) (i) PLS-DA score plot and (ii) loading plot of PLS-DA of serum samples from the normal control, OVA model, DSP and AST using TWDS groups based on UPLC-QTOF-MS in acquired positive ionization mode (iii) PLS-DA score plot and (iv) loading plot of PLS-DA of serum samples from the normal control, OVA model, DSP group and AST using TWDS groups based on UPLC-QTOF-MS in acquired negative ionization mode. Red squares highlighted in (ii) were variable with VIP >1.5